



A01-31264

AIAA 2001-2837

**Assessment of Reynolds Stress Predictions
by Two-Equation Turbulence Models**

Krishnendu Sinha

University of Minnesota and Army High
Performance Computing Research Center
Minneapolis, MN

Ivan Marusic, Graham V. Candler
Aerospace Engineering and Mechanics
University of Minnesota

**31st AIAA Fluid Dynamics
Conference and Exhibit**

11-14 June 2001 / Anaheim, CA

Assessment of Reynolds Stress Predictions by Two-Equation Turbulence Models

Krishnendu Sinha*, Ivan Marusic†, Graham V. Candler‡

Aerospace Engineering and Mechanics* †‡

Army High Performance Computing Research Center* †

University of Minnesota, Minneapolis, MN 55455

Abstract

In this paper, we evaluate the $k - \epsilon$ and $k - \omega$ turbulence models in terms of their accuracy in predicting the Reynolds shear stress in equilibrium boundary layers under arbitrary streamwise pressure gradients. The models are tested against the theoretical formulation of Perry *et al.* (1994) which is based on the law of the wall and law of the wake formulation of the mean velocity profile. Using this formulation, we study the effect Reynolds number and pressure gradient has on the eddy viscosity distribution in the boundary layers flows. In the viscous sub-layer and the buffer layer of zero-pressure gradient boundary layers, the normalized eddy-viscosity, ν_T^+ , is found to be independent of the Reynolds number. A damping function is derived for the $k - \epsilon$ model from the theoretical value of ν_T^+ in the sub-layer and buffer layer, and is used to evaluate several low Reynolds number versions of the $k - \epsilon$ model. In the defect layer, log layer and beyond, the ratio of ν_T^+ to the Reynolds number based on the friction velocity is found to be self-similar, which is consistent with the theoretical formulation. Also, there is a strong influence of the pressure gradient on the distribution of ν_T^+ in this region. The $k - \epsilon$ model prediction is found to be close to the theoretical values of ν_T^+ for favorable and mild adverse gradient flows, whereas the $k - \omega$ model works better for strong adverse pressure gradient cases.

1. Introduction

Reynolds stresses play an important role in all turbulent flows. It represents the effect of turbulent fluctuations on the mean momentum transfer in the flow. In the Reynolds averaged Navier-Stokes (RANS) formulation, the key responsibility of a turbulence model

is to predict the Reynolds stresses correctly. Different turbulence models employ different modeling techniques to obtain the Reynolds stresses.¹ Most algebraic, one-equation and two-equation models formulate the Reynolds stresses in terms of a turbulent eddy-viscosity, which is computed either directly or indirectly from other turbulent and mean flow quantities. On the other hand, second-order closure models directly solve modeled transport equations for the stresses. The one- and two-equations models are used widely for practical applications, mainly because they have a good balance of versatility and simplicity compared to other models. Among two-equation models, the $k - \epsilon$ and $k - \omega$ turbulence models are commonly used. These models solve modeled transport equations for the turbulent kinetic energy, k , and its dissipation rate, ϵ , or the specific dissipation rate, $\omega = \epsilon/k$. The eddy viscosity, ν_T , is then computed in terms of k , ϵ and ω .

Turbulence models are based on various modeling assumptions. Also, there are several constants and empirical damping functions in these models that are generally calibrated to experimental or direct numerical simulation (DNS) data of some simple flows, for example, zero pressure gradient boundary layers, free shear layers, etc. When applied to more complex practical flows, the validity of some of these assumptions and calibrations limit the performance of a turbulence model. For example, it is well known that the $k - \epsilon$ model fails to predict boundary layer flows under strong adverse pressure gradient, and most models have difficulty in predicting non-equilibrium turbulent flows. In this paper, a turbulent boundary layer is referred to as being in equilibrium if there is approximate self-similarity in the mean velocity profiles. Thus, testing of these models for a wide range of flows is very important. It leads to a better understanding of the limitations of each model and also suggests ways to improve them.

The $k - \epsilon$ and $k - \omega$ turbulence models have been tested against a range of experimental test flows,^{1,2,3} where the predictions of the turbulence models are

*Postdoctoral Associate, Member AIAA

†Assistant Professor, Member AIAA

‡Professor, Senior Member AIAA

Copyright © 2001 by Krishnendu Sinha. Published by the American Institute of Aeronautics and Astronautics, Inc. with permission.

compared mostly to measurements of the mean velocity profiles and the skin friction coefficient. These comparisons, however, may not be enough to test the modeling of the Reynolds stresses in these flows. This is because two flows with the same skin friction coefficient and same velocity profile can have drastically different Reynolds stress profiles.⁴ Therefore, in order to assess the accuracy of the model predictions of the Reynolds stress, we need Reynolds stress data from the experiments. This is a severe restriction, because Reynolds stress measurements are available for very few flows,⁵ and secondly, the measurements of the Reynolds stress have limited accuracy.

An alternative to experiments is DNS, where the Reynolds stresses can be computed very accurately and used for model evaluation. There are several works in this direction – Rodi and Mansour,⁶ Sarkar and So,⁷ Sinha *et al.*,⁸ etc. However, DNS data are limited to flows at Reynolds number, Re , much lower than what is encountered in practical applications. Therefore, the results obtained from DNS based testing has limited application. Most of the works cited above use the DNS data to study the modeling of the Reynolds stresses in the low Re region close to a solid wall.

Testing of turbulence models using experimental or DNS data is possible only for the test flows for which data is available. This restricts the evaluation of the models to a limited number of test cases. If we assume that a flow is defined in terms of several parameters, for example, pressure gradient, Reynolds number, equilibrium parameter, etc., then these test cases correspond to a limited number of test points in the whole parameter space. The information obtained from these tests is not sufficient to get a comprehensive assessment of the models over the whole range of flow conditions. In this regard, the approach presented in the paper is very useful, wherein the Reynolds shear stress can be obtained theoretically for a boundary layer which is two-dimensional in the mean, under a wide range of flow conditions. The formulation is based on the assumption that the mean streamwise velocity follows the classic log-layer, law of the wake form.⁹ This velocity profile is then used to obtain the Reynolds shear stress across the boundary layer by integrating the mean momentum and continuity equations. Thus, for a given set of parameters discussed above, the Reynolds stress is obtained theoretically and is used to evaluate the $k - \epsilon$ and $k - \omega$ turbulence models.

The paper is organized as follows. The theoretical formulation is presented in Section 2, where the procedure to obtain the Reynolds shear stress and the eddy viscosity for a given set of flow parameters is out-

lined. We then validate the approach in Section 3 by comparing to experimental and DNS data of several test flows. This is followed by model testing in Section 4, where the Reynolds shear stress predicted by the $k - \epsilon$ and $k - \omega$ turbulence models are compared to the theoretical profiles for different flow conditions. Here, we focus on equilibrium boundary layers under different pressure gradients and at different Reynolds numbers. The testing is done in three parts. First, we test the models in the log layer and study the effect of Re and pressure gradient on the eddy viscosity. Second, we look at the viscous sub-layer and the buffer layer, and test the modeling of the low Re effects on the Reynolds shear stress in this region. Lastly, the defect layer is analyzed to study the effect of pressure gradient, and the turbulence models are evaluated for several conditions. The results from these model evaluations are summarized in Section 5, along with some comments about future work in this direction.

2. Formulation

We use the analysis developed by Perry *et al.*¹⁰ to obtain the Reynolds stress distribution in general two-dimensional turbulent boundary layers. The basis of the analysis is the assumption that the mean velocity profile follows Coles⁹ logarithmic law of the wall and law of the wake formulation, given by

$$\frac{u}{u_\tau} = \frac{1}{\kappa} \log \left(\frac{yu_\tau}{\nu} \right) + A + \frac{\Pi}{\kappa} W_c(\eta, \Pi), \quad (1)$$

where u is the mean stream-wise velocity, $u_\tau = \sqrt{\tau_0/\rho}$ is the friction velocity, τ_0 is the wall shear stress, ρ is the density, κ is the Karman constant ($=0.41$), ν is the kinematic viscosity, y is the wall-normal coordinate, A is the universal law of the wall constant ($=5.1$), Π is Coles wake factor, W_c is Coles wake function, and $\eta = y/\delta$, where δ is the boundary layer thickness. We use the wake function proposed by Jones *et al.*,¹¹

$$W_c(\eta, \Pi) = 2\eta^2(3 - 2\eta) - \frac{1}{\Pi} \frac{\eta^3}{3}. \quad (2)$$

The form (1) assumes that the logarithmic law of the wall is valid right down to the wall, and thus neglects the near-wall viscous effects. In order to include the viscous sublayer and the buffer layer, we replace the log-layer part in Eq. (1) by Reichardt's formula,^{11,12} such that the overall velocity profile is given by,

$$\frac{u}{u_\tau} = f_1(y^+) + \frac{\Pi}{\kappa} W_c(\eta, \Pi), \quad (3)$$

where

$$f_1(y^+) = \frac{1}{\kappa} \log(1 + \kappa y^+) + \left(A - \frac{\log(\kappa)}{\kappa} \right) \times \left[1 - \exp\left(\frac{-y^+}{11}\right) - \frac{y^+}{11} \exp(-0.33y^+) \right]. \quad (4)$$

The validity of this assumption for the mean velocity profile will be shown in the next section.

The velocity defect form of the mean velocity profile (3) is given by,

$$\frac{U_e - u}{u_\tau} = f(\eta, \Pi, S), \quad (5)$$

where U_e is the free-stream velocity, and

$$f(\eta, \Pi, S) = f_1(Re_\tau) - f_1(Re_\tau \eta) + \frac{\Pi}{\kappa} W_c(1, \Pi) - \frac{\Pi}{\kappa} W_c(\eta, \Pi). \quad (6)$$

Here, $Re_\tau = u_\tau \delta / \nu$ is the Reynolds number based on friction velocity (also referred to as the Karman number), $y^+ = u_\tau y / \nu$ is the wall-normal coordinate in wall-units, and is related to η as,

$$y^+ = Re_\tau \eta. \quad (7)$$

It is to be noted that the boundary layer thickness is defined as,

$$\delta = \frac{\delta^*}{C_1} S, \quad (8)$$

where δ^* is the displacement thickness,

$$C_1 = \int_0^1 f(\eta, \Pi, S) d\eta, \quad (9)$$

and S is defined as,

$$S = \frac{U_e}{u_\tau} = \left(\frac{2}{C_f} \right)^{1/2}, \quad (10)$$

where C_f is the local skin friction coefficient,

$$C_f = \frac{\tau_0}{\frac{1}{2} \rho U_e^2}. \quad (11)$$

Using Eq. (3), it can be shown that S , Re_τ and Π are uniquely related as

$$S = f_1(Re_\tau) + \frac{\Pi}{\kappa} W_c(1, \Pi). \quad (12)$$

It is assumed that the mean flow is steady and two-dimensional, and that the stream-wise derivatives of

normal stresses can be neglected. Thus, the mean continuity and streamwise momentum equations are given by

$$\frac{\partial u}{\partial x} + \frac{\partial v}{\partial y} = 0, \quad (13)$$

$$u \frac{\partial u}{\partial x} + v \frac{\partial u}{\partial y} = -\frac{1}{\rho} \frac{dP}{dx} + \frac{1}{\rho} \frac{\partial \tau}{\partial y}, \quad (14)$$

where v is the mean wall-normal velocity component, and x is the stream-wise coordinate, P is the free-stream static pressure and τ is the local effective shear stress given by,

$$\frac{\tau}{\rho} = -\overline{u'v'} + \nu \frac{\partial u}{\partial y}. \quad (15)$$

Here, $\nu \partial u / \partial y$ is the viscous contribution and $-\overline{u'v'}$ is the Reynolds (kinematic) shear stress, where u' and v' are the fluctuating components of velocity in the x - and y -directions, respectively, and the overbar represents Reynolds averaging.

Using the velocity defect-form (5) to integrate the continuity and momentum equations, Perry and Marusic¹³ obtained the result

$$\tau^+ = \frac{\tau}{\tau_0} = g_0(\eta, \Pi, S) + g_1(\eta, \Pi, S)\zeta + g_2(\eta, \Pi, S)\beta, \quad (16)$$

where

$$\zeta = S \delta \frac{d\Pi}{dx}$$

will be referred to as the equilibrium parameter, and

$$\beta = \frac{\delta^*}{\tau_0} \frac{dP}{dx}$$

is the Clauser parameter. The functions g_0 , g_1 and g_2 can be generated quite easily by using *Mathematica* or any equivalent package, or by numerical integration. The normalized Reynolds stress can, thus, be obtained as

$$\frac{-\overline{u'v'}}{u_\tau^2} = \frac{\tau}{\tau_0} + \frac{1}{Re_\tau} \frac{\partial f}{\partial \eta}, \quad (17)$$

and the normalized eddy-viscosity is given by

$$\nu_T^+ = \frac{\nu_T}{\nu} = -1 - \frac{\tau^+ Re_\tau}{(\partial f / \partial \eta)}. \quad (18)$$

Thus, τ^+ and ν_T^+ are functions of five parameters, namely, η , Π , S , β and ζ , and can be evaluated theoretically for any two-dimensional boundary layer flow once these parameters are specified.

3. Validation

In this section, we present comparison of shear stress profiles computed from Eq. (16) with experimental and DNS data of flows described in Table 1. The first flow corresponds to the DNS of a favorable pressure gradient boundary layer of Spalart,¹⁴ and was used to validate the above formulation by Jones *et al.*¹¹ The remaining test cases are by Marusic and Perry,⁴ and they correspond to different stream wise locations of a boundary layer developing under non-equilibrium adverse pressure gradient (the flow number in Table 1 corresponds to the x -location in the experiment). The value of β and Re_τ for each flow is also given in Table 1 along with the value of Π that fits the respective velocity profile.

To validate the formulation presented in Section 2, we first look at the underlying assumptions. The main assumption is that the mean velocity profile has the logarithmic law of the wall and law of the wake form given in Eq. (1). Coles⁹ compiled experimental data for boundary layers from different sources to show that the above assumption is valid. Also, Reichardt's formula for the viscous sub-layer and the buffer layer (4) has been shown to compare well with experimental data.¹² To elucidate the point, we present the mean velocity profiles of the flows listed in Table 1 (Fig. 1). We see that the formula (3) fits the experimental or DNS data points very well.

The analysis also assumes that the stream-wise derivative of the normal stresses is negligible compared to the contribution of the shear stress, which is valid in boundary layers not close to separation, and the formulation is applicable only to flows which are two-dimensional in the mean. Fig. 2 shows the comparison of the computed results with the experimental or DNS data of the test flows. We see that the formula (16) matches reasonably well with the experimental data of Marusic and Perry.⁴ Spalart's DNS data is also reproduced very closely by the formula (17).

Flow	β	Π	Re_τ	Symbol
Sink flow	-0.59	0	550	\triangleright
1200	0.0	0.57	978	\circ
1800	0.65	0.85	1162	∇
2240	1.45	1.38	1195	\square
2640	2.90	2.01	1260	∇
2880	4.48	2.62	1271	\triangleleft
3080	7.16	3.37	1252	\diamond

Table 1. Test flows used for validating the formulation in Section 2.

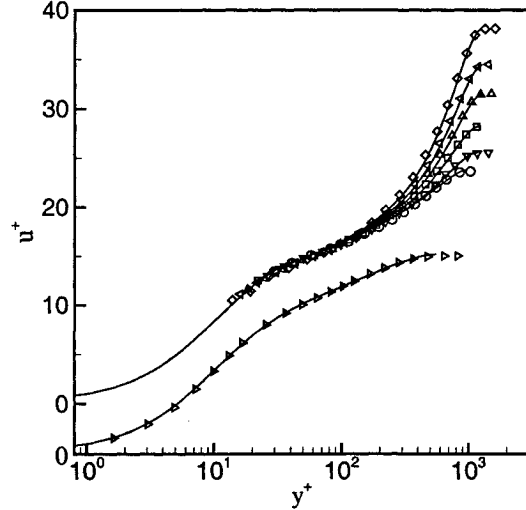


Figure 1. Mean velocity profiles of the flows listed in Table 1. Comparison of formula (3) with the experimental or DNS data points.

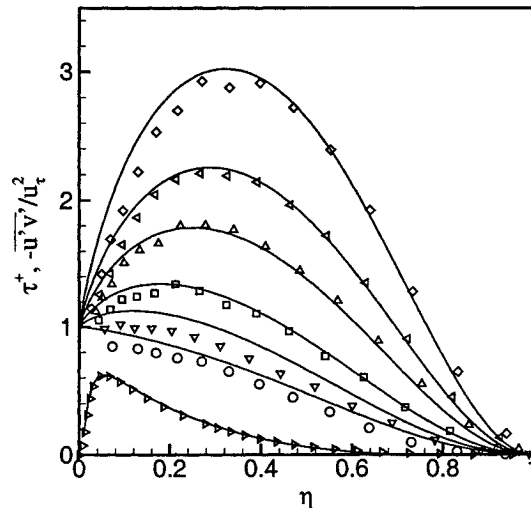


Figure 2. Comparison of τ^+ computed from Eq. (16) for the flows by Marusic and Perry (1995) with the experimental data. The Reynolds shear stress computed for Spalart's sink flow is also compared with the DNS data.

The Reynolds stress and eddy viscosity distribution obtained from Eqs. (17) and (18), respectively, depend on the velocity profile. Therefore, the results may depend on the values of the parameters that define the velocity profile, namely, κ , A and Π . The value of these parameters are obtained by fitting to experimental or DNS data, and therefore have some uncertainty. For example, reported values of κ in the literature range from approximately 0.38 to 0.43 for experimental boundary layers.^{15,16} The value of Π for zero pressure gradient is nominally taken to be about 0.55, but

it may vary between 0.45 and 0.65.¹⁷ Similarly, there is some uncertainty in the value of the log-layer constant, A . Here, we study the sensitivity of the results presented in the paper to the values of these constants.

Fig. 3(a) shows the distribution of ν_T^+ in a zero pressure gradient boundary layer at $Re_\tau = 10000$ for values of $\kappa = 0.38, 0.41$ and 0.43 . We see that there is small sensitivity of ν_T^+ to the value of κ , and the peak ν_T^+ changes by less than 7% from the $\kappa = 0.41$ curve. Similarly, Fig. 3(b) shows that the peak ν_T^+ value changes by less than 5% for values of Π in the range 0.45 to 0.65 as compared to $\Pi = 0.55$. Finally, it is expected that there will be very little sensitivity of the result to the value of A , because it has negligible contribution in the velocity defect formulation. Thus, the overall sensitivity of the eddy viscosity to the value of the constants used in the velocity profile is small.

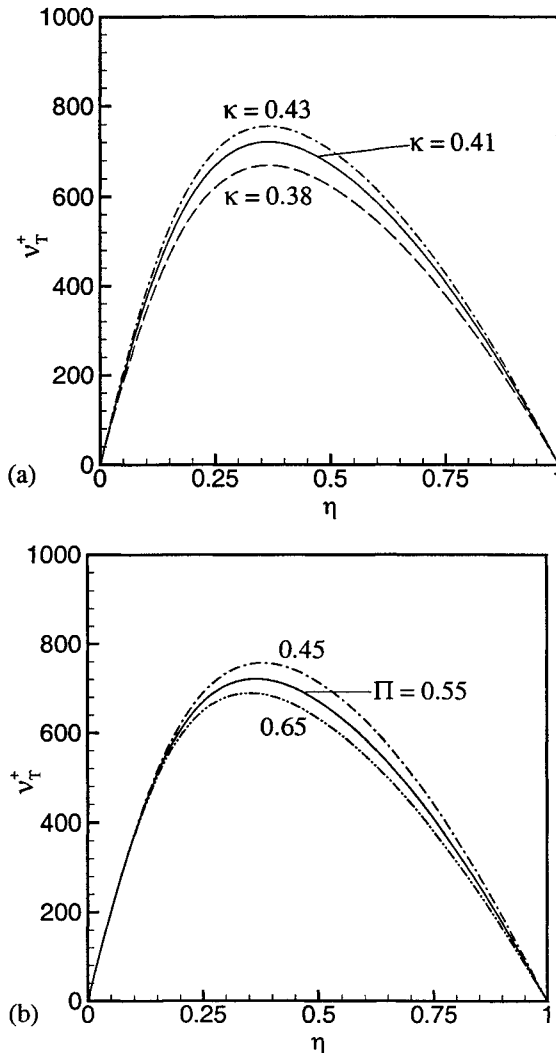


Figure 3. Sensitivity of ν_T^+ to variations in the value of the constants that define the mean velocity profile – (a) κ , and (b) Π .

4. Results

In this section, we use the formulation presented in Section 2 to study the effect of Reynolds number and pressure gradient on equilibrium boundary layers ($\zeta = 0$). The eddy viscosity computed using formula (18) for these boundary layers is compared to what is predicted by the $k - \epsilon$ and $k - \omega$ models. The results are presented in three parts – log layer, viscous sublayer and buffer layer, and defect layer.

Log-layer

We first look at the effect of Re on the eddy viscosity distribution in the log-layer of zero-pressure gradient boundary layers. Figure 4 shows the variation of ν_T^+ as a function of y^+ in the log layer of boundary layers at different values of S , which correspond to different $Re_{\delta^*} = U_e \delta / \nu$ (Table 2). Here, we consider the log-layer to be nominally valid for $y^+ \geq 100$; $y/\delta < 0.15$ (following Spalart)¹⁸. Thus, the log-layer extends to higher y^+ for higher values of S , or higher values of Re_{δ^*} . It can be seen from Fig. 4 that ν_T^+ for each S is close to the $\nu_T^+ = \kappa y^+$ curve (line with symbols) at $y^+ \simeq 100$, and they deviate from this limiting curve at higher y^+ . The deviation of ν_T^+ from κy^+ at a given y^+ is smaller for the higher Re flows than that of the lower Re cases. This suggests that in the log-layer $\nu_T^+ \rightarrow \kappa y^+$ as $Re_\tau \rightarrow \infty$. This is, however, not true, because if we look at the whole log-layer for each flow, the deviation from $\nu_T^+ = \kappa y^+$ at the outer edge of the layer is comparable at different Re_τ . Also, even for high enough Reynolds numbers, these curves do not collapse. Thus, we can conclude that ν_T^+ is not a function of y^+ alone in the log-layer. Instead, if we plot the quantity ν_T^+ / Re_τ as a function of η , then all the curves for different Re_{δ^*} are seen to be identical (Fig 5). Thus,

$$\nu_T^+ = Re_\tau \mathcal{F}(\eta) = Re_\tau \mathcal{F}(y^+ / Re_\tau). \quad (19)$$

This result can also be derived using Eqs (6), (16) and (18). It can also be seen from Fig. 5 that ν_T^+ deviates substantially from the $\nu_T^+ = \kappa y^+$ curve, near the outer edge ($\eta \simeq 0.15$). Note that there is a small deviation from the $\nu_T^+ = \kappa y^+$ curve for $y^+ < 100$ (Fig. 4). This corresponds to the viscous sublayer and the buffer layer. We will study these regions in detail later.

Wilcox¹ gives the values of k , ϵ and ω in the log-layer as obtained by solving the model equations. Thus, it is shown that both the $k - \epsilon$ and $k - \omega$ models predict $\nu_T^+ = \kappa y^+$, where the value of κ as obtained from the $k - \epsilon$ and $k - \omega$ models are 0.433 and 0.41,

S	Re_τ	Re_{δ^*}
26	2444	7821
27	3684	11789
28	5552	17768
29	8368	26777
30	12610	40352
31	19002	60807

Table 2. Value of S , Re_τ and Re_{δ^*} corresponding to the zero pressure gradient flows shown in Fig. 4.

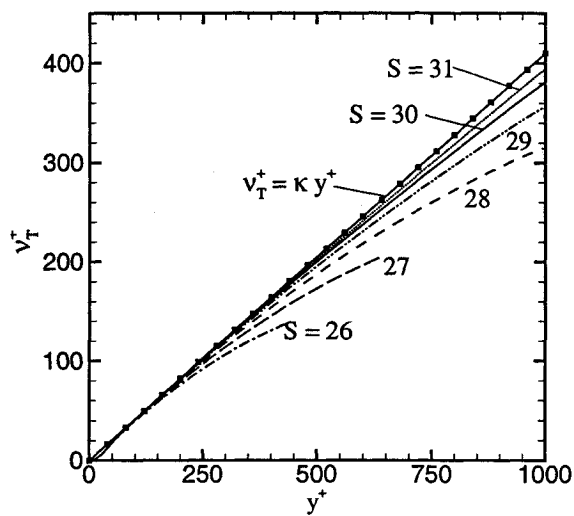


Figure 4. Variation of ν_T^+ with y^+ in the log layer of boundary layers at zero pressure gradient.

respectively. This linear behavior corresponds to the limiting curve shown in Fig. 4, and it matches ν_T^+ only near the lower edge of the log-layer. As pointed above, the deviation from this limiting curve predicted by the models at the outer edge of the log-layer is substantial at any Re . Moreover, it can be seen from Eq. (19) that ν_T^+ is a function of y^+ as well as the Reynolds number. The latter dependence is ignored by the turbulence models.

We next study the effect of pressure gradient on the distribution of eddy viscosity in the log-layer. Fig. 6 shows ν_T^+ as a function of y^+ in several flows at different adverse and favorable pressure-gradients that were experimentally studied by East *et al.*¹⁹ The limiting curve $\nu_T^+ = \kappa y^+$ is also shown for reference. The different curves are identified by the corresponding Clauser parameter values. We see that ν_T^+ for the adverse pressure gradient flows are much higher than the zero pressure gradient case ($\beta = 0$), whereas the favorable pressure gradient flows have lower ν_T^+ .

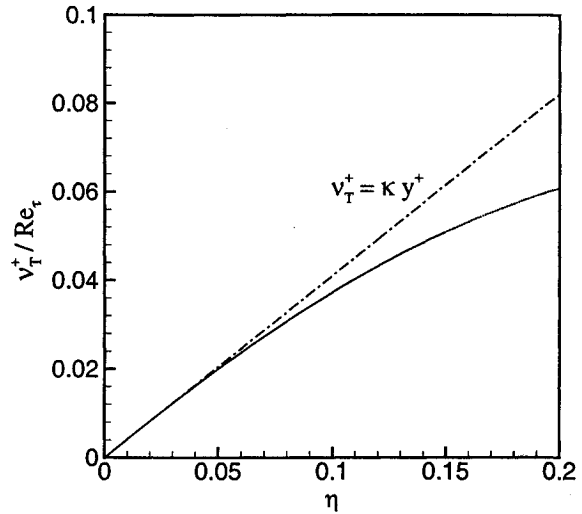


Figure 5. Variation of ν_T^+/Re_τ with η in the log layer of boundary layers at zero pressure gradient. Range of S values, shown in Fig. 4, are considered.

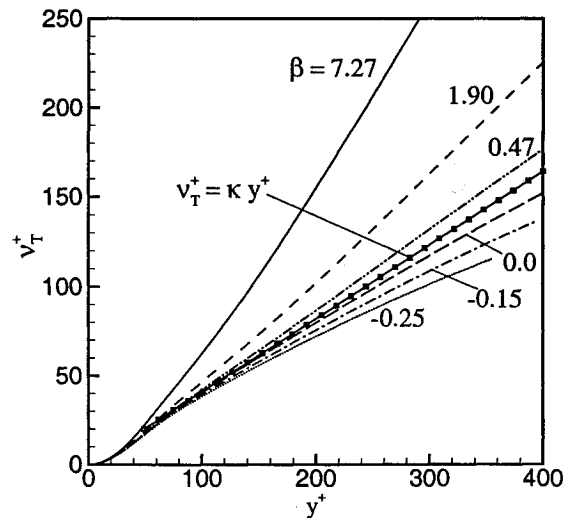


Figure 6. Variation of ν_T^+ with y^+ in the log layer of boundary layers with pressure gradient by East *et al.*¹⁹

Wilcox²⁰ used perturbation analysis to obtain the solution of the $k - \omega$ equations in the log layer for non-zero pressure gradients. Thus, the eddy-viscosity as predicted by the model is given by,

$$\nu_T^+ = \kappa y^+ \left(\frac{1 + 1.16 \phi y^+}{1 - 0.30 \phi y^+} \right), \quad (20)$$

where

$$\phi = \frac{\nu}{\rho u_\tau^3} \frac{dP}{dx},$$

is a small parameter. Fig. 7 shows the comparison of the above formula to ν_T^+ curves for some of the flows

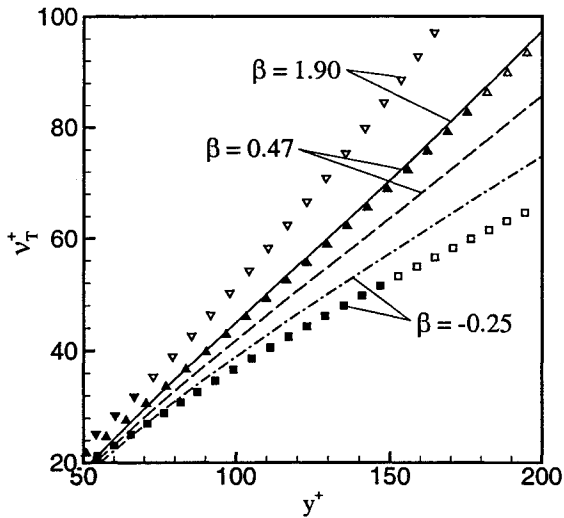


Figure 7. Evaluation of the $k - \omega$ model in the log layer of boundary layers with pressure gradient by East *et al.*¹⁹ The lines correspond to the theoretical values, whereas the $k - \omega$ formula (20) are shown by symbols.

presented in Fig. 6. Here, lines represent the theoretical values computed from Eq. (18), and the symbols correspond to ν_T^+ obtained from Eq. (20). Note that Eq. (20) is derived by assuming that $\phi y^+ \ll 1$ so that the terms involving higher orders of ϕy^+ can be neglected. This sets an upper limit to the value of y^+ , say y_{max}^+ , for which the formula is valid. In Fig. 7, we use solid symbols in the range $y^+ < y_{max}^+$ and open symbols beyond that. Comparing the theoretical values to the model predictions for each flow, we see that Eq. (20) predicts the theoretical ν_T^+ reasonably well in the range of its validity (solid symbols), although the prediction is lower than theory for the favorable pressure gradient flow and higher than theory for the adverse pressure gradient cases. Note that the region $\phi y^+ \ll 1$ in which Eq. (20) is valid, is very limited for stronger pressure-gradients (for example, $\beta = 1.90$ case). Thus, we need to include the higher order terms in Eq. (20) to evaluate the model at higher y^+ .

Extending the procedure followed by Wilcox,²⁰ we look for solutions of the form,

$$\begin{aligned} \frac{\partial u}{\partial y} &= \frac{u_\tau}{\kappa y} [1 + u_1 \phi y^+ + u_2 (\phi y^+)^2 + \dots], \\ k &= \frac{u_\tau^2}{\sqrt{\beta^*}} [1 + k_1 \phi y^+ + k_2 (\phi y^+)^2 + \dots], \\ \omega &= \frac{u_\tau}{\sqrt{\beta^*} \kappa y} [1 + \omega_1 \phi y^+ + \omega_2 (\phi y^+)^2 + \dots]. \end{aligned} \quad (21)$$

By substituting these into the simplified momentum and $k - \omega$ equations for the log-layer,¹ the values of the coefficients (u_1 , k_1 , etc.) can be evaluated. Solving

for the first order terms, we get

$$u_1 = -0.48, \quad k_1 = 1.16, \quad \omega_1 = -0.32,$$

which match the values quoted by Wilcox.²⁰ For the second order terms, we get

$$u_2 = -1122.9, \quad k_2 = 1.22, \quad \omega_2 = 1121.9.$$

In the flows by East *et al.*,¹⁹ $\phi = \mathcal{O}(10^{-3})$, and in the log-layer, $y^+ \geq 100$, so that

$$u_2 (\phi y^+)^2 \geq 10^2 u_1 (\phi y^+)$$

and

$$\omega_2 (\phi y^+)^2 \geq 10^2 \omega_1 (\phi y^+).$$

Thus, the second order terms cannot be neglected. In fact, some of the third and fourth order coefficients are found to be $\mathcal{O}(10^3)$ and $\mathcal{O}(10^6)$, respectively, and therefore these terms cannot be neglected. We may even need to keep terms of order higher than four. Thus, the first order solution is not accurate and the validity of Eq. (20) is highly questionable. A similar analysis of the $k - \epsilon$ model resulted in a solution, where the higher order terms again could not be neglected. Thus, the procedure based on the form of the solution (21) is found to be not suitable for these cases.

Viscous sublayer

Figure 8 shows the variation of ν_T^+ with y^+ in the viscous sub-layer and the buffer layer of boundary layers at zero pressure gradient. The curves correspond to values of S between 26 and 32, alternatively Re_τ between 2000 and 28000. The limiting curve in the log-layer, $\nu_T^+ = \kappa y^+$, is also shown for comparison. We see that all the different Re curves collapse together in the viscous sublayer and buffer layer, but they show some variation in the log-layer. Specifically, ν_T^+ for the high Re_τ cases are very close to the κy^+ value, and ν_T^+ for the lower Re_τ flows are somewhat lower than κy^+ . Note that the lower Re curves never quite reach the limiting log-layer value.

In the $k - \epsilon$ turbulence model, the eddy-viscosity is modeled in terms of the turbulent kinetic energy, k , and its dissipation rate, ϵ . In non-dimensional form,

$$\nu_T^+ = c_\mu f_\mu \frac{k^+}{\epsilon^+}, \quad (22)$$

where $k^+ = k/u_\tau^2$ and $\epsilon^+ = \epsilon/\nu_\tau^3$. c_μ is a model constant and is generally accepted to be 0.09, and f_μ is a damping function. $f_\mu = 1$ in the log

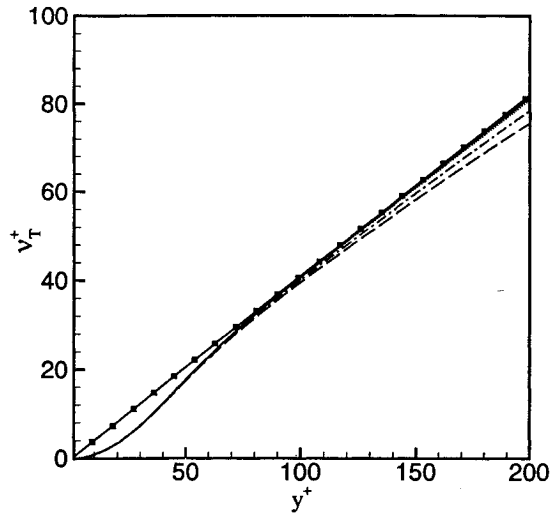


Figure 8. Variation of ν_T^+ with y^+ in the viscous sub-layer and the buffer layer of boundary layers at zero pressure gradient at different Reynolds numbers.

layer and is lower than unity in the viscous sub-layer and the buffer layer. Different versions of the $k - \epsilon$ model prescribe different forms of the damping function. The idea is to obtain f_μ from ν_T^+ computed from Eq. (18) and compare it to the model damping functions. It is to be noted that the $k - \omega$ model does not use any damping function.

In order to compute f_μ , we need to solve the modeled transport equations for k^+ and ϵ^+ . A simplified form of the equations presented by Jones and Launder²¹ for the viscous sub-layer through the log-layer is given by,

$$\nu_T^+ \left(\frac{\partial u^+}{\partial y^+} \right)^2 - \epsilon^+ - \frac{1}{2k^+} \left(\frac{\partial k^+}{\partial y^+} \right)^2 + \frac{\partial}{\partial y^+} \left[\left(1 + \frac{\nu_T^+}{\sigma_k} \right) \frac{\partial k^+}{\partial y^+} \right] = 0, \quad (23)$$

$$c_1 f_1 k^+ \left(\frac{\partial u^+}{\partial y^+} \right)^2 - c_2 f_2 \frac{\epsilon^{+2}}{k^+} + 2\nu_T^+ \left(\frac{\partial^2 u^+}{\partial y^{+2}} \right)^2 + \frac{\partial}{\partial y^+} \left[\left(1 + \frac{\nu_T^+}{\sigma_\epsilon} \right) \frac{\partial \epsilon^+}{\partial y^+} \right] = 0, \quad (24)$$

where c_1 , c_2 are model constants, f_1 and f_2 are empirical damping functions to account for the near wall effects on the ϵ -equation, and σ_k and σ_ϵ are corresponding Prandtl numbers.

$$c_1 = 1.44, \quad c_2 = 1.92, \quad \sigma_k = 1.0, \quad \sigma_\epsilon = 1.3,$$

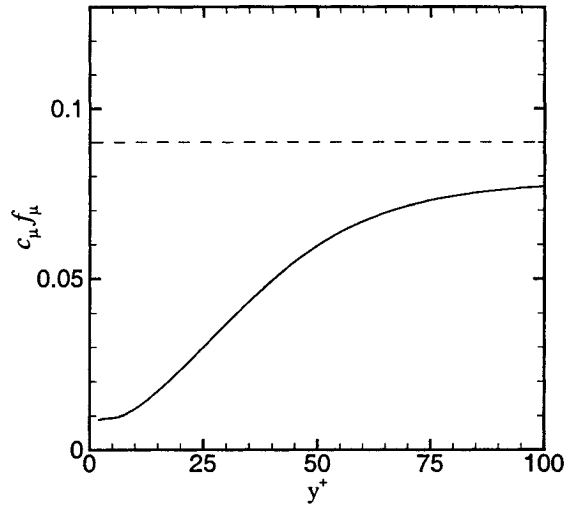


Figure 9. Variation of $c_\mu f_\mu$ with y^+ in the viscous sub-layer and the buffer layer of boundary layer at zero pressure gradient at $Re_\tau = 1400$.

$$f_1 = 1, \quad f_2 = 1 - 0.3 \exp(-Re_T^2),$$

where $Re_T = k^{+2}/\epsilon^+$ is the turbulent Reynolds number. The convection terms are neglected in the above equations. The boundary condition at the wall are

$$k^+ = \epsilon^+ = 0, \quad (25)$$

and in the log-layer ($\nu_T^+ \gg 1$), and the solutions to Eqs. (23) and (24) are

$$k^+ = \frac{1}{\sqrt{c_\mu}}, \quad \epsilon^+ = \frac{1}{\kappa y^+}, \quad \nu_T^+ = \kappa y^+. \quad (26)$$

We solve the $k - \epsilon$ equations (23) and (24) subjected to the boundary conditions (25) and (26) using a fourth order Runge-Kutta method. We apply the log-layer conditions on k^+ and ϵ^+ , and integrate to the wall, varying $\partial k^+/\partial y^+$ and $\partial \epsilon^+/\partial y^+$ until the wall boundary conditions (25) are satisfied. For the values of ν_T^+ and u^+ , we use the results obtained from Eq. (18) and (3), respectively, for the case of $\beta = 0$ and $Re_\tau = 1400$. Thus, we get the profiles of k^+ and ϵ^+ in the viscous sub-layer through the log layer, which can now be used along with Eq. (22) to get,

$$c_\mu f_\mu = \frac{\nu_T^+ \epsilon^+}{k^{+2}}, \quad (27)$$

which is shown in Fig. 9. We see that $c_\mu f_\mu$ reaches an asymptotic value in the log-layer ($y^+ \geq 100$), whereas

Model	Code	f_μ
Launder-Sharma ²²	LS	$\exp(-3.4/(1 + 0.02Re_T)^2)$
Chien ²³	CH	$1 - \exp(-0.0115y^+)$
Lam-Bremhorst ²⁴	LB	$[1 - \exp(-0.0165y^*)]^2 (1 + 20.5/Re_T)$
Shih-Mansour ²⁵	SM	$1 - \exp(-6 \times 10^{-3}y^+ - 4 \times 10^{-4}y^{+2} + 2.5 \times 10^{-6}y^{+3} - 4 \times 10^{-9}y^{+4})$
Nagano-Tagawa ²⁶	NT	$[1 - \exp(-y^+/26)]^2 (1 + 4.1/Re_T^{3/4})$
Rodi-Mansour ⁶	RM	$1 - \exp(-2 \times 10^{-4}y^+ - 6.5 \times 10^{-4}y^{+2})$
Myong-Kasagi ²⁷	MK	$(1 + 3.45/\sqrt{Re_T}) [1 - \exp(-y^+/70)]$

Table 3. Damping function, f_μ , used in different low Re versions of the $k - \epsilon$ turbulence model. Here, $y^+ = u_\tau y / \nu$, $y^* = k^{1/2} y / \nu$ and $Re_T = k^2 / \nu \epsilon$.

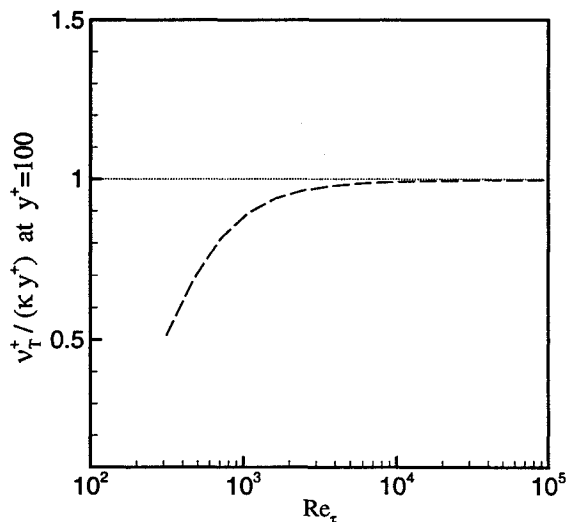


Figure 10. The ratio $\nu_T^+ / (\kappa y^+)$ at $y^+ = 100$ as a function of Re_τ for boundary layers with zero pressure gradient.

it is comparatively lower in the viscous sub-layer and the buffer layer ($y^+ < 100$) due to the damping effect of the wall that reduces the eddy viscosity. In the limit $y^+ \rightarrow 0$,

$$k^+ = \mathcal{O}(y^2), \quad \epsilon^+ = \mathcal{O}(y), \quad \nu_T^+ = \mathcal{O}(y^3),$$

so that $c_\mu f_\mu = \mathcal{O}(1)$ and reaches a constant value.

The value of $c_\mu f_\mu$ in the log-layer ($y^+ \simeq 100$) is about 0.077, which is lower than the generally accepted value of $c_\mu = 0.09$ ($f_\mu = 1$). This is mainly due to the fact that the flow considered here is at a relatively low Reynolds number ($Re_\tau = 1400$), for which ν_T^+ is considerably lower than κy^+ in the log layer (Fig. 8).

Similar low values of $c_\mu f_\mu$ are also reported by Rodi and Mansour⁶ using DNS data of low Re boundary layers. In order to study this Reynolds number effect, we plot the ratio of ν_T^+ at $y^+ = 100$ to the limiting value κy^+ for different Re_τ flows (Fig. 10). It can be seen that the ratio $(\nu_T^+ / \kappa y^+)_{y^+=100}$ asymptotes to 1 for high values of Re_τ , and it drops lower than unity near $Re_\tau = 1000$. If we assume that $f_\mu = 1$ in the log-layer ($y^+ \simeq 100$), then

$$\left(\frac{\nu_T^+}{\kappa y^+} \right)_{y^+=100} = \frac{c_\mu}{0.09},$$

and thus the curve shown in Fig. 10 can be interpreted as the decrease in the value of c_μ from 0.09 at low Reynolds numbers. On the other hand, if we assume that $c_\mu = 0.09$, then the asymptotic value of f_μ at large y^+ is a function of the Reynolds number and is given by the ratio $(\nu_T^+ / \kappa y^+)_{y^+=100}$ in Fig. 10.

The damping functions prescribed by some of the commonly used versions of the $k - \epsilon$ model are listed in Table 3. The damping functions are calibrated to reach a value of unity at large y^+ . Thus, they are valid for high Re flows (for which $\nu_T^+ \simeq \kappa y^+$ at $y^+ \simeq 100$), and do not account for the low Re effect discussed above. Thus, a comparison of the model damping functions with the theoretical f_μ computed using Eq. (27) for a high Re flow will assess the accuracy of the models. However, in the absence of theoretical f_μ for a high Re flow at this point in time, we re-scale the f_μ for $Re_\tau = 1400$ by using a value of c_μ smaller than 0.09 such that $f_\mu = 1$ at $y^+ \simeq 100$. The results are shown in Fig. 11, where the solid symbols correspond to the f_μ obtained from Eq. (27) and

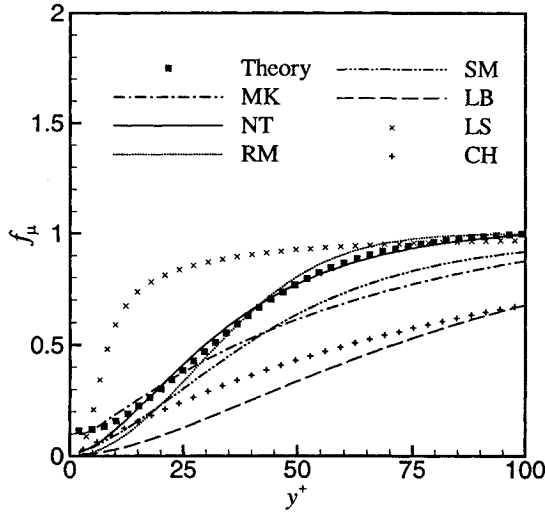


Figure 11. Evaluation of different model damping functions (Table 3) against the theoretically obtained f_μ for a boundary layer at zero pressure gradient at $Re_\tau = 1400$.

the different models are identified by the codes given in Table 3. Also, it is to be noted that f_μ obtained theoretically is based on the Jones and Launder model, and some of the other models in Table 3 have a slightly different formulation (see Ref. 6 for details). However, based on the DNS data presented by Rodi and Mansour,⁶ we expect that these differences will result in very little variation in the theoretically computed f_μ for $y^+ > 10$. Therefore, the f_μ obtained from Eq. (27) using the Jones and Launder formulation of the $k - \epsilon$ turbulence model can be used to evaluate different model damping functions. From the model testing in Fig. 11, we see that the model by NT compares very well with the theory, and the model by RM is also reasonably good. The damping functions by MK and SM under-predict the theoretical curve. The damping function by LS rises too quickly but is lower than f_μ from theory for $y^+ > 80$. Finally, the damping functions of the models LB and CH are much lower than the theoretical f_μ and reach the value of unity far too slowly.

Defect Layer

The defect layer is the outer part of a boundary layer. It is the region above the viscous buffer layer where Reynolds number similarity of the velocity defect holds. Fig. 12 shows the ratio ν_T^+/Re_τ in zero pressure gradient boundary layers at $Re_\tau = 1000$ through 50000. We see that ν_T^+/Re_τ for all the different Re_τ cases are identical.

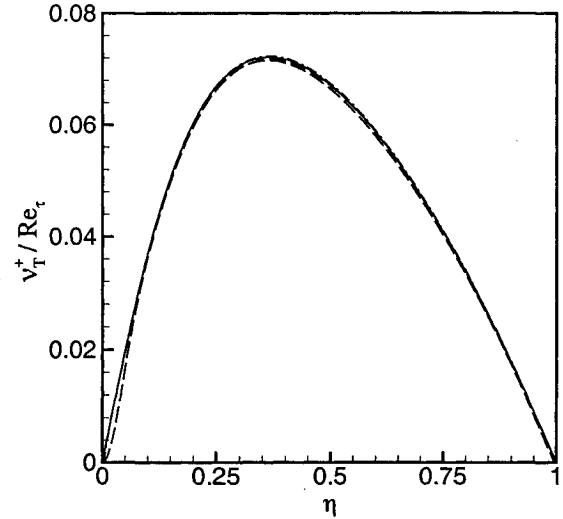


Figure 12. Variation of ν_T^+/Re_τ with η in boundary layers at zero pressure gradient for $Re_\tau = 1000$ through 50000.

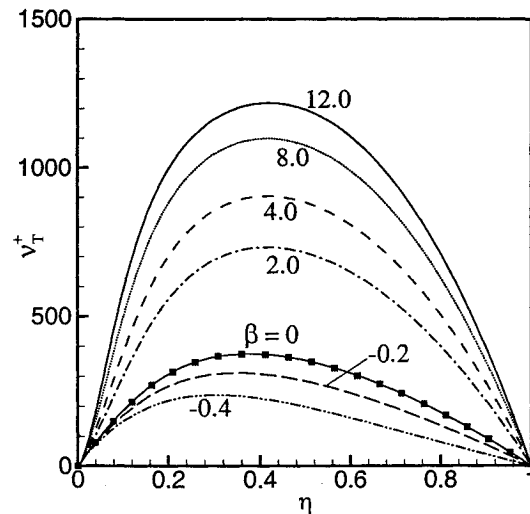


Figure 13. Variation of ν_T^+ with η in boundary layers at zero, favorable and adverse pressure gradients ($Re_\tau = 5000$).

Fig. 13 shows the variation of ν_T^+ with η in equilibrium boundary layers ($\zeta = 0$) at $Re_\tau = 5000$ under different pressure gradients. The curves are identified by the corresponding values of β . We see that ν_T^+ is larger in the adverse pressure gradient cases ($\beta > 0$) as compared to the zero-pressure gradient flow ($\beta = 0$). Also, the rate of increase in ν_T^+ with β is higher for small values of β (~ 1) than at higher values of β (~ 10). For favorable pressure gradient flows, ν_T^+ is lower than the zero pressure gradient value.

Wilcox¹ presents perturbation analysis to solve the $k - \epsilon$ and $k - \omega$ turbulence model equations in the defect layer of boundary layers under equilibrium pres-

sure gradient conditions. We use this analysis to compare the turbulence models to the ν_T^+ data presented above. A brief description of the analysis follows. The streamwise and wall-normal coordinates are scaled as

$$\xi = \frac{x}{L} \quad \text{and} \quad \psi = \frac{y}{\Delta(x)},$$

where L is a characteristic streamwise length scale and $\Delta = U_e \delta^* / u_\tau$. The streamwise velocity, the eddy viscosity, and k , ϵ and ω are transformed as,

$$\begin{aligned} u(x, y) &= U_e - u_\tau U(\psi), \\ \nu_T(x, y) &= U_e \delta^* N(\psi), \\ k(x, y) &= \frac{u_\tau^2}{\sqrt{\beta^*}} K(\psi), \\ \epsilon(x, y) &= \frac{u_\tau^3}{\Delta} E(\psi), \\ \omega(x, y) &= \frac{u_\tau}{\sqrt{\beta^*} \Delta} W(\psi), \end{aligned}$$

where β^* is a model constant. The mean momentum equation and the turbulence model equations are solved to obtain U , N , K , E and W as functions of the normalized distance from the wall, ψ . Note that

$$N(\eta) = \frac{\nu_T^+(\eta)}{Re_{\delta^*}}, \quad (28)$$

where $\eta = \psi / \psi_{\text{edge}}$. The solutions for different values of β are computed using the software provided by Wilcox,¹ and the ν_T^+ profiles, thus obtained, are compared to the corresponding theoretical values.

Figure 14(a) shows the variation of $\nu_T^+(\eta)/Re_{\delta^*}$ for different values of β (2, 4, 6, 8, 10 and 12), as obtained from Eq. (18). The curves correspond to boundary layers at $Re_\tau = 5000$. We see that the value of ν_T^+/Re_{δ^*} is lower for stronger adverse pressure gradient (higher β). The values of N obtained by solving the $k-\epsilon$ and $k-\omega$ model equations for different values of β are shown in the figure by solid and open symbols, respectively. We note that there is very little variation in N for different β . Thus, the models do not predict the variation in ν_T^+/Re_{δ^*} as obtained from theory. Furthermore, the prediction of the $k-\epsilon$ model is higher than the theoretical curves, whereas the values of N as predicted by the $k-\omega$ model lie close to the theoretical curve for $\beta = 8$. On the whole, the $k-\epsilon$ prediction is close to the theoretical ν_T^+/Re_{δ^*} for mild adverse pressure gradient ($\beta \simeq 2$), and the $k-\omega$ model works better for stronger adverse pressure gradient flows ($\beta \simeq 10$).

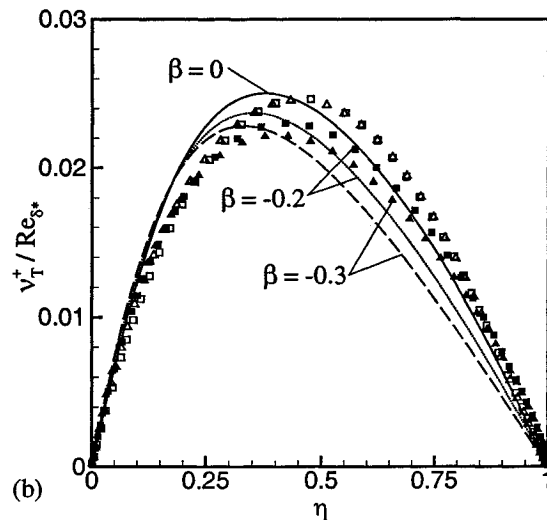
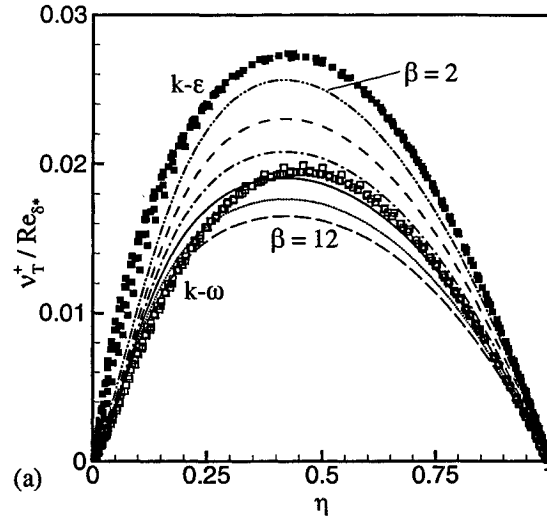


Figure 14. Comparison of ν_T^+/Re_{δ^*} as predicted by $k-\epsilon$ and $k-\omega$ turbulence models to the theoretical curves obtained from Eq. (18) in boundary layers under pressure gradients – (a) adverse and (b) favorable. The solid symbols represent the $k-\epsilon$ model and the open symbols correspond to the $k-\omega$ model. The results obtained from Eq. (18) are shown by lines.

Figure 14(b) shows the variation of $\nu_T^+(\eta)/Re_{\delta^*}$ for different favorable pressure gradient cases ($Re_\tau = 5000$). We see that ν_T^+/Re_{δ^*} from Eq. (18) in the favorable pressure gradient cases is slightly higher than the zero pressure gradient curve for $\eta < 0.15$ which corresponds to the log-layer. However, the trend is reversed for $\eta > 0.15$, where ν_T^+/Re_{δ^*} for $\beta < 0$ is smaller than that for $\beta = 0$, and ν_T^+/Re_{δ^*} at a given η decreases as the magnitude of β increases. N obtained from the turbulence models for $\beta = -0.2$ and -0.3 are also shown in the figure. We see that the values of N obtained from the two models are very similar in the range $0 < \eta < 0.25$, and are reasonably

close to the theoretical curves. However, for larger values of η , N from the $k - \epsilon$ model is lower, and therefore closer to the theoretical curves, than that from the $k - \omega$ model. In addition, the $k - \omega$ results (open symbols) are less sensitive to the change in β than the $k - \epsilon$ model (solid symbols), which reproduces the theoretical trend of ν_T^+ with pressure gradient correctly.

5. Conclusions

In this paper, we evaluate the $k - \epsilon$ and $k - \omega$ turbulence models in terms of their accuracy in predicting the Reynolds shear stress in boundary layers under arbitrary pressure gradients. The model predictions are tested against the Reynolds stress and eddy viscosity computed using the analysis of Perry *et al.*¹⁰ for two-dimensional boundary layers, which is based on the assumption that the mean streamwise velocity follows the logarithmic law of the wall and law of the wake. Using this formulation, we first study the effect of Reynolds number, Re , on the distribution of the eddy viscosity in zero-pressure gradient boundary layers, and then evaluate the modeling of this Re effect. Secondly, we look at the effect of pressure gradient on the eddy viscosity and assess the accuracy of the models in different pressure gradient flows.

The eddy viscosity normalized by the kinematic viscosity, ν_T^+ , in the viscous sub-layer and the buffer layer is found to be independent of the Reynolds number for zero-pressure gradient flows. A damping function, f_μ , is derived for the $k - \epsilon$ model from the theoretical value of ν_T^+ , and the Re dependence of the asymptotic value of f_μ in the log-layer (for large y^+) is studied. Several low Re variations of the $k - \epsilon$ model are evaluated against f_μ obtained from theory. In the defect layer, log-layer and beyond, the ratio of ν_T^+ to Re_τ is found to be self-similar, consistent with the theoretical formulation. The $k - \epsilon$ and $k - \omega$ models predict a linear behavior of ν_T^+ in the log-layer, which is close to the theoretical value in the low y^+ part of the log-layer, but has a substantial discrepancy near the outer edge of the log-layer. There is a strong influence of pressure gradient on ν_T^+ distribution in the defect layer. Comparison of the models with the theory shows that the $k - \epsilon$ model is close to the theoretical value in favorable and mild adverse pressure gradient flows, whereas the $k - \omega$ model works well for strong-adverse pressure gradient cases. Both models, however, fail to reproduce the variation in the ν_T^+ distribution with varying pressure gradient that is predicted by the theory. Thus, the $k - \epsilon$ and $k - \omega$ models could be tested for a wide range of equilibrium turbulent boundary

layers, using the theoretical formulation of Perry *et al.* (1994). Further investigation in this direction will be continued, including the extension of the procedure to non-equilibrium turbulent flows using computational fluid dynamics.

Acknowledgements

This work was sponsored by the Army High Performance Computing Research Center under the auspices of the Department of the Army, Army Research Laboratory cooperative agreement number DAAH04-95-2-0003 / contract number DAAH04-95-C-0008, the content of which does not necessarily reflect the position or the policy of the government, and no official endorsement should be inferred. The second author is supported by the National Science Foundation under grant CTS-9983933.

References

- 1 Wilcox, D.C., *Turbulence Modeling for CFD*, DCW Industries, Inc., La Canada, CA, 1998.
- 2 Patel, V.C., Rodi, W., and Scheurer, G., "Turbulence Models for Near-Wall and Low Reynolds Number Flows: A Review," *AIAA Journal*, Vol. 23, No. 9, 1985, pp. 1308-1319.
- 3 Wilcox, D.C., and Rubesin, M.W., "Progress in Turbulence Modeling for Complex Flow Fields Including Effects of Compressibility," NASA TP-1517, April 1980.
- 4 Marusic, I., and Perry, A.E., "A Wall-Wake Model for the Turbulence Structure of Boundary Layers. Part 2. Further Experiment Support," *Journal of Fluid mechanics*, Vol. 298, 1995, pp. 389-407.
- 5 Smith, P.D. and Jimenez, J., "Two-dimensional Boundary-Layer," *A Selection of Test Cases for the Validation of Large-Eddy Simulations of Turbulent Flows*, AGARD Advisory Report 345, April 1998, pp. 37-42.
- 6 Rodi, W., and Mansour, N.N., "Low Reynolds Number $k - \epsilon$ Modeling with the Aid of Direct Simulation Data," *Journal of Fluid Mechanics*, Vol. 250, 1993, pp. 509-529.
- 7 Sarkar, A., and So, R.M.C., "A Critical Evaluation of Near-Wall Two-Equation Models against Direct Numerical Simulation Data," *Int. J. Heat and Fluid Flow*, Vol. 18, 1997, pp. 197-208.
- 8 Sinha, K., Martin, M.P., and Graham, G.V., "Assessment of the $k - \epsilon$ Turbulence Model for Compressible Flows using Direct Simulation Data," AIAA Paper 2001-0730, Jan. 2001.

- ⁹ Coles, D.E., "The Law of the Wake in the Turbulent Boundary Layer," *Journal of Fluid Mechanics*, Vol. 1, 1956, pp. 191-226.
- ¹⁰ Perry, A.E., and Marusic, I., and Li, J.D., "Wall Turbulence Closure Based on Classical Similarity Laws and the Attached Eddy Hypothesis," *Physics of Fluids*, Vol. 6, 1994, pp. 1024-1035.
- ¹¹ Jones, M.B., and Marusic, I., and Perry, A.E., "Evolution and Structure of Sink-Flow Turbulent Boundary Layers," *Journal of Fluid Mechanics*, Vol. 428, 2001, pp. 1-27.
- ¹² Schlichting, H., *Boundary-Layer Theory*, McGraw-Hill, Inc., 1979.
- ¹³ Perry, A.E., and Marusic, I., "A Wall-Wake Model for the Turbulence Structure of Boundary Layers. Part 1. Extension of the Attached Eddy Hypothesis," *Journal of Fluid mechanics*, Vol. 298, 1995, pp. 361-388.
- ¹⁴ Spalart, P.E., "Numerical Study of Sink Flow Boundary Layers," *Journal of Fluid mechanics*, Vol. 172, 1986, pp. 307-320.
- ¹⁵ Zagarola, M.V., and Smits, A.J., "Mean-Flow Scaling of Turbulent Pipe Flow," *Journal of Fluid mechanics*, Vol. 373, 1998, pp. 33-79.
- ¹⁶ Osterlund, J.M., and Johansson, A.V., and Nagib, H.M., and Hites, M.H., "A Note on the Overlap Region in Turbulent Boundary Layers," *Physics of Fluids*, Vol. 12, No. 1, 2000, pp. 1-4.
- ¹⁷ Coles, D.E., "The Turbulent Boundary Layer in a Compressible Fluid," USAF The Rand Cooperation, Rep. R-403-PR, Appendix A, 1962.
- ¹⁸ Spalart, P.E., "Direct Simulation of a Turbulent Boundary Layer up to $R_\theta = 1410$," *Journal of Fluid Mechanics*, Vol. 187, 1988, pp. 61-98.
- ¹⁹ East, L.F., Sawyer, W.G., and Nash, C.R., "An Investigation of the Structure of Equilibrium Turbulent Boundary Layers," RAE TR-79040, 1979.
- ²⁰ Wilcox, D.C., "Wall Matching, A Rational Alternative to Wall Functions," AIAA Paper 89-0611, Jan. 1989.
- ²¹ Jones, W.P., and Launder, B.E., "The Prediction of Laminarization with a Two-Equation Model of Turbulence," *Int. J. Heat Mass Transfer*, Vol. 15, 1972, pp. 301-314.
- ²² Launder, B.E., and Sharma, B.I., "Application of the Energy Dissipation Model of Turbulence to the Calculation of Flow Near a Spinning Disc," *Lett. Heat Mass Transfer*, Vol. 1, No. 2, 1974, pp. 131-138.
- ²³ Chien, K.Y., "Prediction of Channel and Boundary-Layer Flows with a Low-Reynolds-Number turbulence Model," *AIAA Journal*, Vol. 20, No. 1, 1982, pp. 33-38.
- ²⁴ Lam, C.K.G., and Bremhorst, K.A., "Modified Form of the $k - \epsilon$ Model for Predicting Wall Turbulence," *Journal of Fluid Engineering*, Vol. 103, 1981, pp. 456-460.
- ²⁵ Shih, T-H, and Mansour, N.N., "Modeling of Near Wall Turbulence," In *Engineering Turbulence Modeling and Experiments*, (ed. W. Rodi and E.N. Ganic), Elsevier, 1990, pp. 13-19.
- ²⁶ Nagano, Y., and Tagawa, M., "An Improved $k - \epsilon$ Model for Boundary Layer Flows," *Journal of Fluids Engineering*, Vol. 112, 1990, pp. 33-39.
- ²⁷ Myong, H.K., and Kasagi, N., "A New Approach to the Improvement of $k - \epsilon$ Turbulence Model for Wall-Bounded Shear Flows," *JSME International Journal*, Vol. 33, 1990, pp. 63-72.